626 Journal of Electrical Engineering & Technology Vol. 7, No. 4, pp. 626~635, 2012
http://dx.doi.org/10.5370/JEET.2012.7.4.626

Elimination of Clock Jump Effects in Low-Quality Differential GPS Measurements

Hee-Sung Kim* and Hyung-Keun Lee†

Abstract – Most of single frequency GPS receivers utilize low-quality crystal oscillators. If a low-quality crystal oscillator is utilized as the time reference of a GPS receiver, the receiver's clock bias grows very fast due to its inherent low precision and poor stability. To prevent the clock bias becoming too large, large clock jumps are intentionally injected to the clock bias and the time offset for clock steering purpose. The abrupt changes in the clock bias and the time offset, if not properly considered, induce serious accuracy degradation in relative differential positioning. To prevent the accuracy degradation, this paper proposes an efficient and systematic method to eliminate the undesirable clock jump effects. Experiment results based on real measurements verify the effectiveness of the propose method.

Keywords: GPS, Clock bias, Clock steering, Differential positioning

1. Introduction

Recently, real-time kinematic positioning by single frequency GPS receivers has gained many attentions due to its feasibility for low-cost traffic monitoring, formation flying, precision farming, and structure monitoring.

Rubidium and cesium oscillators are extensively utilized for the precise time synchronization among the GPS satellites since they provide stable and precise timing reference information. Most of commercial GPS receivers, however, utilize crystal oscillators such as temperature compensated crystal oscillators and ovenized crystal oscillators to reduce manufacturing cost.

If a low-quality crystal oscillator is utilized as the timing reference of a GPS receiver, the receiver's clock bias grows very fast due to its inherent low precision and poor stability [1]. To prevent the clock bias becoming too large, clock steering needs to be applied. Though there are differences depending on manufacturers and receiver types, clock steering methods usually adopt two popular methods. One is the continuous steering method [2] and the other is the clock jumping method [3, 4]. Since the clock jumping method requires relatively less hardware resource, it is adopted by many low-cost receivers.

This study is motivated during an attempt to develop a precise relative differential positioning algorithm based on low-cost GPS receivers. In testing a receiver, unacceptable large positioning errors were found periodically in saw-tooth shapes as reported in [5, 6]. This phenomenon did not happen in testing high-quality geodetic-grade receivers. After tracing the source of the problem, it was found that the large positioning errors were synchronized with the abrupt changes in the receiver clock bias, which was caused by the clock jumping method adopted by the receiver firmware. Related to this problem, however, it was hard to find previous study results with detailed explanation or analysis. To expand the utilization of low-quality receivers, it is necessary to study this problem in a rigorous manner.

This paper proposes an efficient and systematic compensation method to eliminate the undesirable clock jump effects occurring in relative differential positioning with low-quality GPS receivers. Based on the finding that large clock jumps affect both the signal reception time and the signal transmission time, the proposed compensation method consists of two steps; reception time compensation and transmission time compensation.

To deal with this topic, this paper is organized as follows. At first, a typical clock steering mechanism which generates periodic clock jumps is explained. Secondly, compensation of the signal reception time is explained. Next, compensation of the signal transmission time is explained. Finally, through three different types of real-measurement experiments, the effectiveness of the proposed compensation method is demonstrated.

2. Clock Steering

To facilitate the explanations from now on, it would be helpful to clarify three terminologies as shown in Fig. 1; time tag, time offset, and clock bias. The time tag indicates the estimated time instant when the measurements are sampled by the receiver. The time tag is decomposed into the integer part and the non-integer part. The non-integer fractional part of the time tag is called as the time offset.

† Corresponding Author: School of Electronics and Telecomm., Korea Aerospace Univ., Korea. (hyknlee@kau.ac.kr)
* School of Electronics and Telecomm., Korea Aerospace Univ., Korea. (hskim07@kau.ac.kr)
Received: March 15, 2011; Accepted: January 10, 2012

The clock bias corresponds to the deviation of the receiver time reference from the GPS time reference. As widely known, the clock bias is usually considered as one of state variables to be estimated. In Fig. 1, t_{rec} and SPL indicate the clock bias sampled by the receiver and the speed of light, respectively.

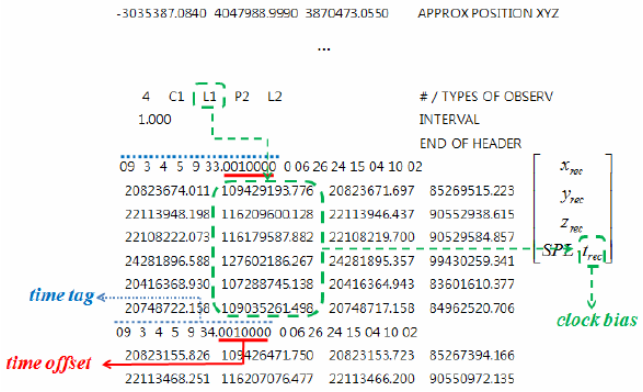

Fig. 1. Discrimination of time tag, time offset, and clock bias in a RINEX-format file logging measurements from a GPS receiver

The fractional parts of the time offset and the clock bias are interchangeable to each other since both of them affect all the GPS measurements. They are equivalent by the opposite sign conventions.

GPS receivers embedding low-quality crystal oscillators usually adopt various clock steering methods. The clock steering methods are largely divided into two categories. One is the continuous steering and the other is the clock jumping. In the continuous steering, the clock bias is monitored and controlled continuously by a feedback mechanism so that it can be bounded within small ranges as shown in Fig. 2. The continuous steering method is adopted by several high-quality geodetic-grade receivers.

In the clock jumping, the clock bias is monitored but not controlled. If the clock bias grows fast in one specific direction and reaches a pre-defined bound, an intentional large clock jump is applied in the opposite direction to prevent further growth. At the same time, to nullify the clock jump effects in the clock bias, the same amount of jump but in the opposite direction is applied to the time offset.

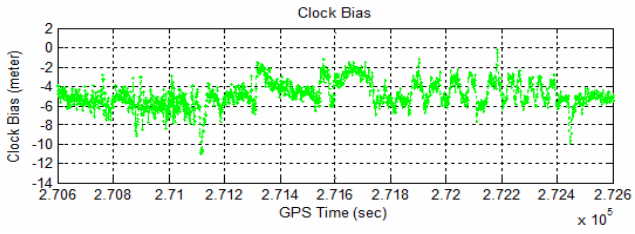

Fig. 2. Clock bias trend by continuous clock steering method

The clock jumping method, in general, causes two different types of misalignments in relative differential positioning; reception time misalignment (RTM) and transmission time misalignment(TTM). The RTM occurs when the time tags or the time offsets of the two receivers are not the same, which means that time tags are not exact integers. Meanwhile, the TTM occurs when the clock biases of the two receivers are different.

3. Compensation of Signal Reception Time

To deal with the RTM in more detail, it is necessary to classify clock jumps adopted by clock steering methods. Table 1 shows four types of clock jumps. Type 1 appears in several high-quality geodetic receivers. Type 2 and Type 3 correspond to the clock jumps occurring at either pseudoranges or time offsets, respectively. Rarely, some commercial receivers adopt Type 2 and Type 3 at the same time. The concurrence of Type 2 and Type 3 is classified as Type 4.

Table 1. Four types of clock jumps

Type	Pseudo-range	Carrier phase	Clock offset
1	Jump	Jump	No jump
2	Jump	No jump	No jump
3	No jump	No jump	Jump
4	Jump	No jump	Jump

Fig. 3 illustrates the time offset and the basic GPS measurements affected by the Type 4 clock jumps. In Fig. 3, intermittent jumps can be found in the time offset trend at regular interval. The intermittent jumps can be divided into two categories whether the time offset can exceed a pre-defined bound or not after a jump in one specific direction is applied. If the time offset is not expected to exceed the pre-defined bound after a jump is applied in the negative (positive) direction as shown in Step 1 of Fig. 3 (b), no jump occurs in pseudorange measurements.

However, when the time offset is expected to exceed the pre-defined threshold value in the negative (positive) direction as shown in Step 2 in Fig. 3(b), a positive (negative) jump value is applied instantaneously to the time offset to maintain the time offset with in the pre-defined threshold value. At the same time, the same amount of negative (positive) value is applied to all the pseudorange measurements to nullify the time offset change.

Considering the most complex Type 4 clock jumps, the compensation of the reception time misalignment is performed by two steps; time offset removal and jump synchronization. The time offset removal begins by intentionally setting the non-zero time offset contained in the time tag to the zero value [7].

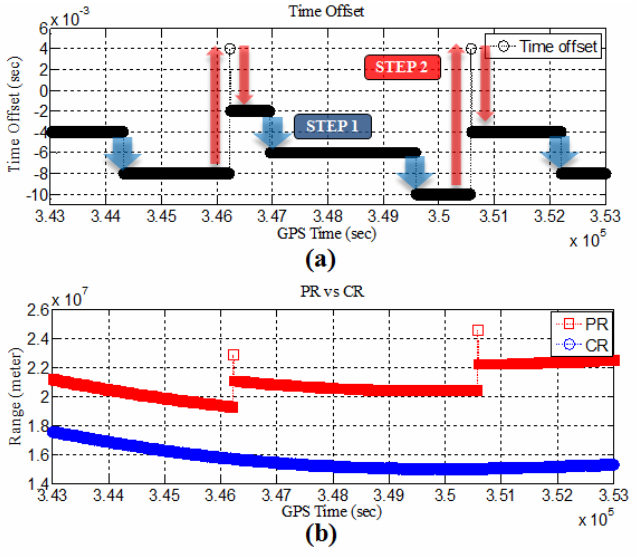

Fig. 3. Uncorrected: (a) time offset; (b) pseudorange and carrier phase measurements affected by clock jumps

$$t_{rec,k} \Leftarrow t_{rec,k} - t_{offset,k} \tag{1}$$

where the symbol " $\Leftarrow$ " denotes substitution, $t_{rec,k}$ denotes the time tag, and $t_{offset,k}$ denotes the time offset at the k-th epoch, respectively. At the same time, since the time offset and the clock bias are equivalent and interchangeable by the opposite sign conventions, the following compensation algorithm is applied to the pseudorange and carrier phase measurements to maintain the clock bias magnitude.

$$\begin{aligned} \tilde{\rho}_k^j &\Leftarrow \tilde{\rho}_k^j - SPL \cdot t_{offset,k} \\ \tilde{\phi}_k^j &\Leftarrow \tilde{\phi}_k^j - SPL \cdot t_{offset,k} \end{aligned} \tag{2}$$

where $\tilde{\rho}_k^j$ and $\tilde{\phi}_k^j$ denotes the pseudorange and carrier phase measurements with respect to the j-th satellite at the k-th epoch, respectively. The compensation by (2) is applied to all the measurements with respect to the visible satellites.

As shown in Fig. (c), some receivers do not show the same amount of clock jumps in the pseudorange and carrier phase measurements. It can make channel-wise fault detection or interpretation of the measurements difficult [8]. To prevent the difficulty, the discrepancy in the jump magnitudes is eliminated in the jump synchronization after the time offset removal by (2).

The jump synchronization utilizes the fact that the difference of jump magnitudes in pseudorange and carrier phase measurements are usually integer multiples of a unit jump magnitude. The unit jump magnitude depends on receiver type and can be determined by pre-processing a set of logged measurements. Once the unit jump magnitude is determined in advance, the following compensation can be applied in real-time.

Testing Clock Jump Occurrence :

$$\left|(\tilde{\rho}_k^j - \tilde{\rho}_{k-1}^j) - (\tilde{\phi}_k^j - \tilde{\phi}_{k-1}^j)\right| > SPL \cdot u_{jump}$$

Compensation of Clock Jump Effects :

$$\begin{aligned} N_{jump,k} &= round\left\{\frac{1}{SPL \cdot m_k \cdot u_{jump}} \sum_{j=1}^{m_k}\left[(\tilde{\rho}_k^j - \tilde{\rho}_{k-1}^j) - (\tilde{\phi}_k^j - \tilde{\phi}_{k-1}^j)\right]\right\} \\ N_k &= N_{jump,k} + N_{k-1} \\ \text{corrected } \tilde{\phi}_k^j &= \tilde{\phi}_k^j - SPL(t_{offset,k} - N_k \cdot u_{jump}) \end{aligned} \tag{3}$$

where u_{jump} denotes the unit jump magnitude, $N_{jump,k}$ denotes the incremental integer multiples, N_k denotes the total integer multiples, and m_k denotes the number of visible satellites at the k-th epoch. The compensation by (3) is also applied to all the measurements with respect to the visible satellites.

Fig. 4 illustrates the clock bias (upper plot) and the measurement trends (lower plot) after the RTM compensation based on (1), (2), and (3). It can be seen in Fig. 4 that the all the jumps occurring in clock bias, pseudorange, and carrier phase are synchronized, which corresponds to the Type 1 jump characteristics occurring in high-quality geodetic receivers. In Fig. 4, the trend of corrected time offset is not depicted since it is maintained zero at all the time.

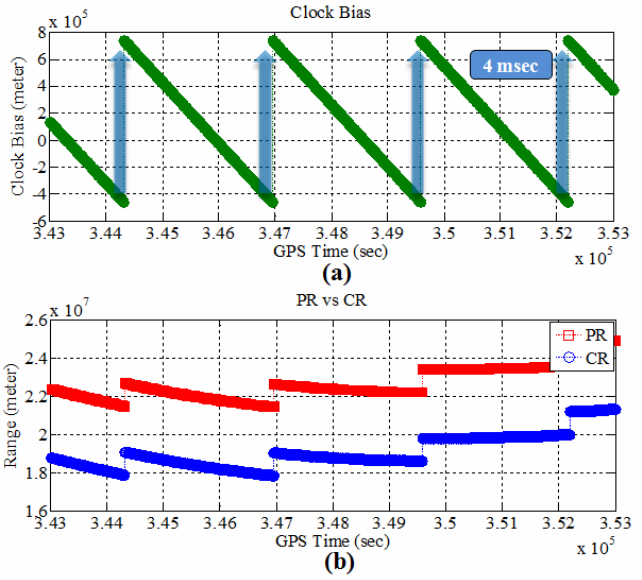

Fig. 4. Corrected: (a) clock bias; (b) pseudorange and carrier phase measurements

4. Compensation of Signal Transmission Time

It is well known that differential clock bias can be eliminated by double-differencing technique. However, this

can only be accomplished if the magnitude of the differential clock bias is relatively small. The TTM compensation explained in this section needs to be applied when there is a large differential clock bias in relative differential positioning and timing.

The effects of the TTM are illustrated in Fig. 5 and Fig. 6 where

$i \in \{u, r\}$: receiver index for user or reference
$t_{i,rec,k}$: estimated signal reception time (time tag)
t_k : true signal reception time
$t_k^{j,i}$: true signal transmission time
ε_k^j : atmospheric delay
$b_{i,k}$: receiver clock bias (in meter)
b_k^j : satellite clock bias (in meter)

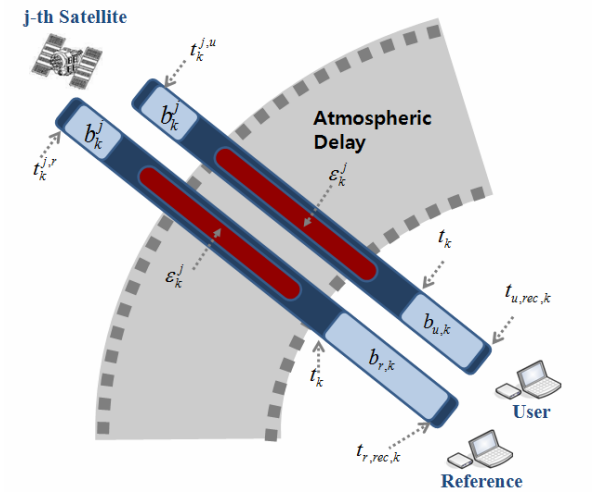

Fig. 5. Comparison of the pseudorange measurements obtained by two receivers installed at the same location

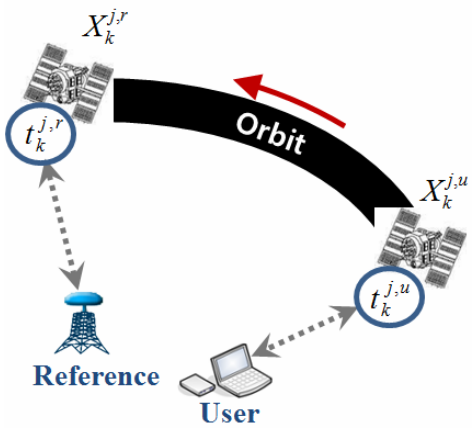

Fig. 6. Different positions of the same satellite due to different signal transmission times

Fig. 5 shows the geometry of two different pseudoranges sampled by two different receivers installed at the same location (zero baseline). For the given condition, all the error sources except the clock bias are the same. As shown in Fig. 5, if the time tags of the two receivers are the same but the receiver clock biases are different, the difference in receiver clock biases generates a difference in signal transmission times, which causes the TTM. The TTM causes a large difference in the computed positions of the same satellite. The different satellite positions cause, in turn, the different LOS vectors as shown in Fig. 6.

If the TTM is not compensated properly, receiver positioning errors become unacceptably large as will be shown later in the experiment. To investigate how the positioning accuracy deteriorates due to the TTM, all the time-related parameters need to be clarified. For this purpose, a pseudorange measurement obtained by the i-th receiver with respect to the j-th satellite at the k-th epoch is modeled as follows [9].

$$\begin{aligned} \tilde{\rho}_{i,k}^j &= SPL \cdot \left[t_{i,rec,k}^j - (t_k^{j,i} + \delta t_k^{j,i}) \right] + \varepsilon_k^j + v_{i,k}^j \\ t_{i,rec,k} &= t_k + \delta t_{i,rec,k} \\ t_k^{j,i} &= t_k - \frac{r_{i,k}^j}{SPL} \end{aligned} \tag{4}$$

where
$\tilde{\rho}_{i,k}^j$: pseudorange measurement
$v_{i,k}^j$: measurement noise
$\delta t_{i,rec,k}^j$: receiver clock bias (in sec)
$\delta t_k^{j,i}$: satellite clock bias (in sec)
$r_{i,k}^j$: geometric range

$$\tilde{\rho}_{i,k}^j = r_{i,k}^j + \left[b_{i,k} - b_k^j \right] + \varepsilon_k^j + v_{i,k}^j \tag{5}$$

The geometric range $r_{i,k}^j$ between the i-th receiver and the j-th satellite can be expressed as follows.

$$\begin{aligned} r_{i,k}^j &= (e_{i,k}^j)^T [X_k^{j,i} - X_{i,k}] \\ e_{i,k}^j &= \frac{1}{\left\| X_k^{j,i} - X_{i,k} \right\|} [X_k^{j,i} - X_{i,k}] \end{aligned} \tag{6}$$

By combining (5) and (6), the pseudorange measurements with respect to the j-th satellite obtained by both receivers can be modeled as (7) and (8), respectively.

$$\begin{aligned} \tilde{\rho}_{u,k}^j &= (e_{u,k}^j)^T [X_k^{j,u} - X_{u,k}] \\ &\quad + [b_{u,k} - b_k^j] + \varepsilon_k^j + v_{u,k}^j \end{aligned} \tag{7}$$

$$\begin{aligned} \tilde{\rho}_{r,k}^j &= (e_{r,k}^j)^T [X_k^{j,r} - X_{r,k}] \\ &\quad + [b_{r,k} - b_k^j] + \varepsilon_k^j + v_{r,k}^j \end{aligned} \tag{8}$$

where
$X_k^{j,u}$ / $X_k^{j,r}$: position of the j-th satellite at the k-th epoch when the navigation signal is

transmitted to the user / reference receiver

$X_{u,k}$ / $X_{r,k}$: position of the user / reference receiver

It should be noted again that $\tilde{\rho}^j_{u,k}$ and $\tilde{\rho}^j_{r,k}$ are related to the different signal transmission times $t^{j,u}_k$ and $t^{j,r}_k$.

Fig. 7 shows the configuration of relative differential positioning when there is no TTM and the baseline between the two receivers is close enough (medium or short baseline). Since it can be assumed $e^j_{u,k} \cong e^j_{r,k}$ and $X^{j,u}_k \cong X^{j,r}_k$ in this case, a single-differenced pseudorange measurement can be modeled as follows.

$$\begin{aligned}\tilde{\rho}^j_{ru,k} &= \tilde{\rho}^j_{r,k} - \tilde{\rho}^j_{u,k} \\ &= (e^j_{u,k})^T [X_{u,k} - X_r] + b_{ru,k} + v^j_{ru,k}\end{aligned} \tag{9}$$

where

$b_{ru,k}$: differential clock bias

$v^j_{ru,k}$: differential measurement noise

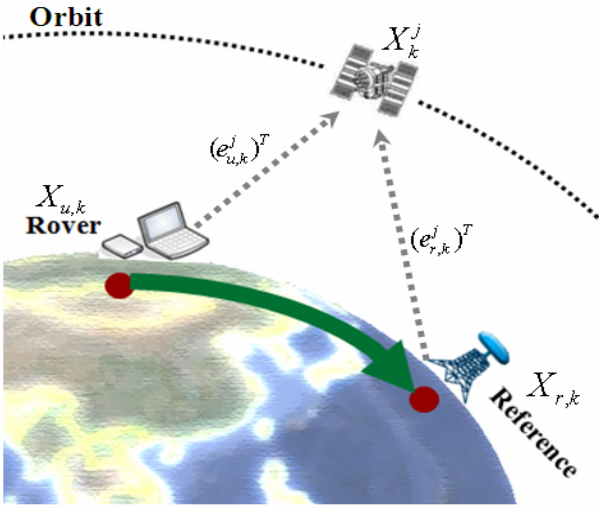

Fig. 7. Configuration of relative positioning if there is no large differential clock bias

On the contrary, if there is a TTM, the following conditions hold.

$$e^j_{u,k} \neq e^j_{r,k}, \quad X^{j,u}_k \neq X^{j,r}_k \tag{10}$$

In this case, it is necessary to consider more general geometry for relative differential positioning. For this purpose, Fig. 8 is utilized instead of Fig. 7 to analyze and compensate the TTM. Based on the geometry shown in Fig. 8, a differential pseudorange measurement affected by a TTM can be modeled as follows.

$$\begin{aligned}\tilde{\rho}^j_{ru,k} &= (e^{j,r}_{r,k})^T [X^{j,r}_k - X_r] \\ &\quad - (e^{j,u}_{u,k})^T [X^{j,u}_k - X_{u,k}] + b_{ru,k} + v^j_{ru,k}\end{aligned} \tag{11}$$

where

$e^{j,r}_{ru,k}$ / $e^{j,u}_{ru,k}$: LOS vector from the reference / user receiver to the j-th satellite

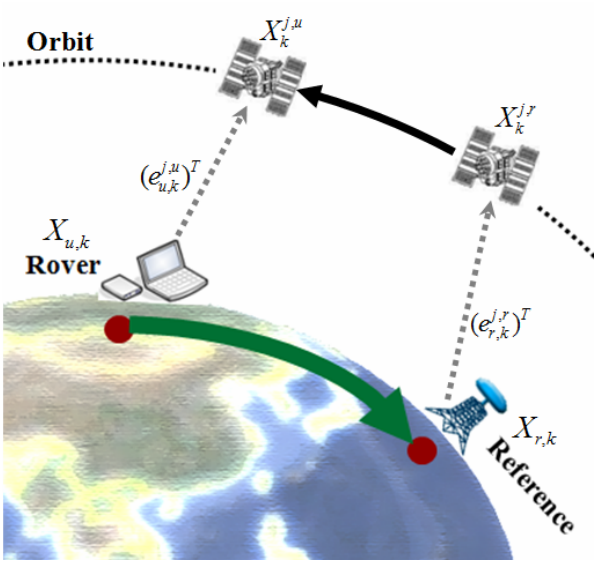

Fig. 8. Configuration of relative positioning considering large differential clock bias

In (11), the position X_r of the reference receiver is exactly known. In relative differential positioning, it is not the absolute position $X_{u,k}$ but the relative baseline ($X_{u,k} - X_{r,k}$) that needs to be estimated. To estimate the baseline accurately, a correction term $\chi_{ru,k}$ needs to be computed as follows.

$$\chi^j_{ru,k} = (e^{j,r}_{r,k})^T [X^{j,r}_k - X_r] - (e^{j,u}_{u,k})^T [X^{j,u}_k - X_r] \tag{12}$$

Based on $\chi_{ru,k}$ computed by (12), the TTM compensation is applied to the original differential pseudorange $\tilde{\rho}^j_{ru,k}$ to obtain the compensated pseudorange $\rho^j_{ru,k}$.

$$\begin{aligned}\rho^j_{ru,k} &= \tilde{\rho}^j_{ru,k} - \chi^j_{ru,k} \\ &= (e^{j,u}_{u,k})^T [X_{u,k} - X_r] + b_{ru,k} + v^j_{ru,k}\end{aligned} \tag{13}$$

By a similar procedure, the original differential carrier phase $\tilde{\phi}^j_{ru,k}$ can also be compensated as follows to obtain the compensated differential carrier phase $\phi^j_{ru,k}$.

$$\begin{aligned}\phi^j_{ru,k} &= \tilde{\phi}^j_{ru,k} - \chi^j_{ru,k} \\ &= (e^{j,u}_{u,k})^T [X_{u,k} - X_r] + b_{ru,k} + \lambda N^j_{ru,k} + v^j_{ru,k}\end{aligned} \tag{14}$$

As shown in (13) and (14), the compensated pseudorange and carrier phase measurements are related to the relative baseline ($X_{u,k} - X_{r,k}$).

To summarize, a large difference in clock biases between the user and reference receivers causes a TTM. The TTM,

in turn, causes a large difference in LOS vectors. The large difference in LOS vectors finally causes a large error in user position estimation. To compensate the TTM, a correction term needs to be computed based on (12). If the correction term is applied to the differential pseudorange and carrier-phase measurements based on (13) and (14), the large positioning error caused by the TTM can be eliminated.

5. Experiment

To verify the effectiveness of the proposed method, three experiments were performed. Throughout all the experiments, data processing was applied in kinematic mode. For the compensation of undesirable clock jump effects, the time offset values were extracted at first from the reference and user receivers at each epoch as shown in Fig. 9. Then, the proposed compensation method was applied to correct the time tag and the measurements.

For kinematic positioning, the position-domain carrier-smoothed-code filter [10] was utilized since it can provide accurate position estimates in the presence of frequent changes in visible satellites and cycle slips. By the advantage, the effectiveness of the proposed compensation method can be depicted clearly.

To show the flexible applicability of the proposed method, three experiments with different configurations were performed; zero baseline, static medium baseline (39.3km), and kinematic short baseline. In these experiments, Septentrio PolaRx2e, NovAtel DL4-PLUS, u-blox AEK-4T, and Trimble NetRS receivers were utilized. The clock steering methods of the receivers utilized in the experiments are summarized in Table 2.

In the first experiment which corresponds to the zero baseline, a Septentrio PolaRX2e receiver and a u-blox AEK-4T receiver were utilized as the reference and user receivers, respectively. Fig. 10 and Fig. 11 illustrate experiment results.

Table 2. Clock steering methods with respect to the receivers used in experiments

	Receiver Type	Clock Steering
Septentrio PolaRx2e	Dual-frequency	Clock jump (Type 1)
NovAtel DL4-PLUS	Dual-frequency	Continuous clock steering
u-blox AEK-4T	Single-frequency	Clock jump (Type 4)
Trimble NetRS	Dual-frequency	Continuous clock steering
Trimble NetRS	Dual-frequency	Clock jump (Type 3)

Fig. 10(a) shows the clock bias trends of the two receivers. Both receivers adopt the clock jumping method to steer their internal clocks. As summarized in Table 2, the

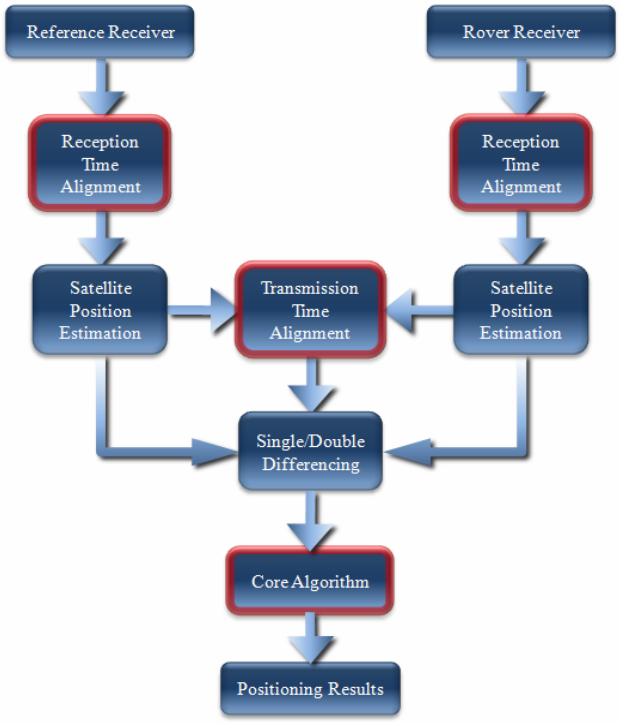

Fig. 9. Data processing procedure for time misalignment compensation

Septentrio PolaRX2e receiver generates Type 1 clock jumps and the u-blox AEK-4T receiver generates the Type 4 clock jumps. To compensate the RTM occurring in Type 4 clock jumps, the compensation algorithm summarized in (3) was applied.

Fig. 10(b) illustrates the position differences of the same satellite due to the TTM between the reference and user receivers. By comparing Fig. 10(a) and (b), it can be seen that the satellite position differences are proportional to the clock bias differences. Fig. 10(c) and (d) show the trends of the elevation angle and the proposed correction term with respect to an arbitrary satellite, respectively. By comparing (b) and (d) of Fig. 10, it can be seen that the time misalignment affects the satellite position differences. In addition, it can be seen that the satellite position differences and elevation angles affect the correction term.

Fig. 11(a) and (b) show the positioning errors of the user receiver with respect to the locally-level NED frame before and after applying the proposed method, respectively. By comparing Fig. 10(b) and Fig. 11(a), it can be verified that large differential clock bias generates large positioning errors. It can also be observed that the discontinuities of positioning errors shown in Fig. 11(a) are synchronized with the clock jumps shown in Fig. 10(a). By comparing Fig. 11(a) and Fig. 11(b), it can be seen that the proposed compensation method eliminates the TTM effects properly. As a result, the maximum position error is reduced from 6 m to 0.02 m, approximately.

The second experiment corresponds to a medium static

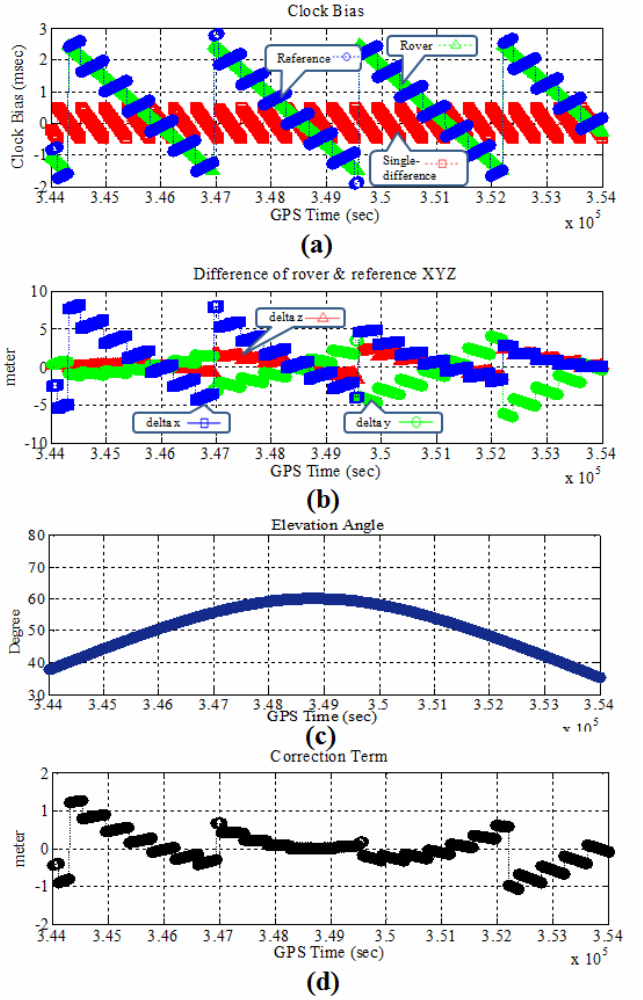

Fig. 10. Zero baseline experiment results: (a) clock bias trends; (b) satellite position differences; (c) satellite elevation angles; (d) correction terms

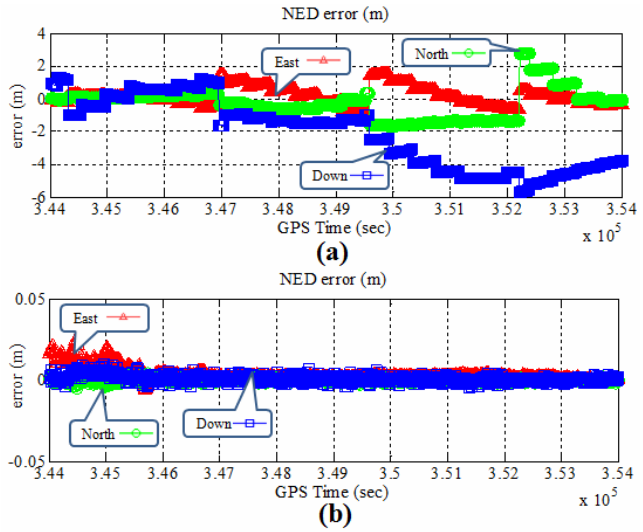

Fig. 11. Zero baseline experiment results: (a) non-compensated positioning error; (b) compensated positioning error

baseline case. In this experiment, the baseline length between the reference and user receiver is approximately 39.3 km. In this experiment, two Trimble NetRS receivers were utilized as the reference and user receivers, respectively. However, the reference receiver adopts the continuous clock steering method referencing external atomic clock and the user receiver adopts the clock jumping method, respectively.

Fig. 12 illustrates the kinematic positioning results for the static baseline. Fig. 12(a), (b), (c), and (d) illustrate the trends of the clock bias, the time offset, and the positioning error before and after the compensation, respectively.

By comparing Fig. 12(a) and (b), it can be observed that the changes in clock bias are accumulated to the time offset since the user receiver adopts the clock jumping method. By comparing Fig. 12(b) and (c), it can also be observed that there is a strong correlation between the differential clock bias and the positioning error before the compensation. The mean and standard deviation of the positioning errors shown in Fig. 12(c) and (d) are summarized in Table 3,

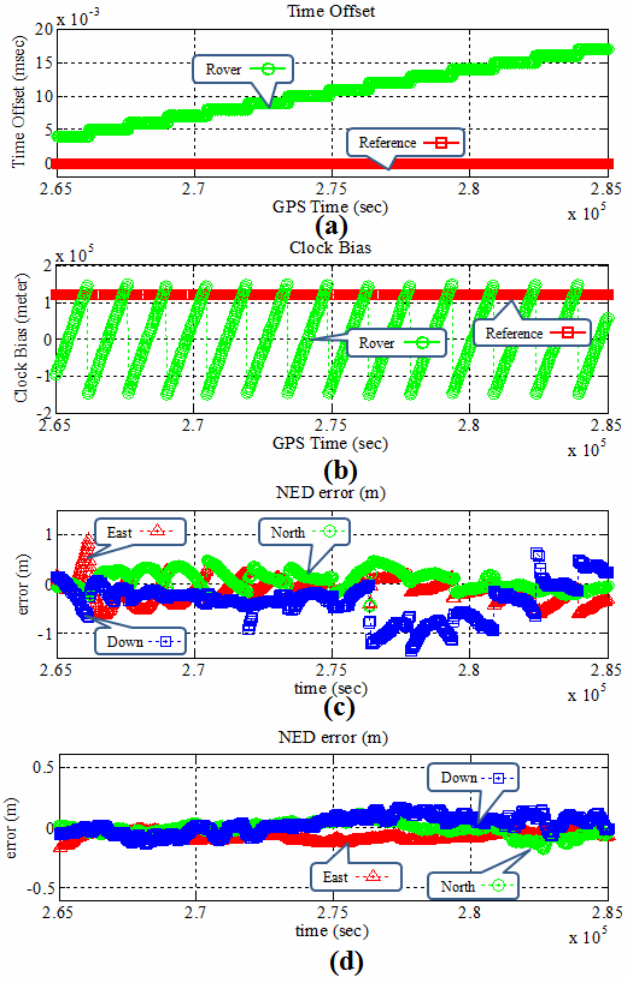

Fig. 12. Medium baseline experiment results: (a) time offset trends; (b) clock bias trends; (c) non-compensated positioning error; (d) compensated positioning error

which shows that the proposed method practically eliminates the RTM and TTM effects even in the medium baseline case. It is also remarkable that cm-level accuracy can be achieved in horizontal plane utilizing low-quality L1 GPS receiver as a rover.

Table 3. Mean and standard deviation values of the positioning error in medium baseline experiment

	Error Mean (m)			Standard Deviation (m)		
	North	East	Down	North	East	Down
Non-Compensated	0.007	-0.044	-0.202	0.453	0.384	0.808
Compensated	-0.014	-0.049	-0.039	0.069	0.060	0.104

The last experiment is purposed to evaluate the performance of the proposed method in kinematic applications. Fig. 13(a) shows the experiment area where the maximum baseline length between the reference and the user receivers is approximately 430 m. Fig. 13(b) shows baseline and velocity trends of moving vehicle. The experiment was performed for 33 minutes (2000 epochs).

In this experiment, a Septentrio PolaRX2e and a NovAtel DL4-PLUS were utilized as the reference and user receiver, respectively. The reference receiver adopts the clock jumping method which generates the Type 1 clock jumps and the user receiver adopts the continuous clock steering method as summarized in Table 1.

In kinematic experiments, it is usually difficult to provide accurate reference trajectory. To solve this problem, the integer solutions generated by two different software packages were utilized for consistency check. Fig. 14 shows the kinematic experiment results. Fig. 14(a) illustrates the clock bias trends. Fig. 14(b), (d), and (f) show the error distance profiles with respect to the locally-level NED frame. Fig. 14(c), (e), and (g) illustrate the reference trajectory by the integer solutions, the estimated trajectory before the compensation, and the estimated trajectory after the compensation, respectively. By comparing Fig. 14(a), (b), (d), and (f), it can be observed again that large positioning errors are caused by large differential clock biases as in the previous experiments. The large differential clock biases shown in Fig. 14(a) are caused by the frequent clock jumps occurring in the reference receiver that adopts the clock jumping method.

Until now, three different experiment results were explained. According to the diversities of the experiments in terms of receiver type, baseline length, and receiver dynamics, it can be verified that the proposed RTM and TTM compensation method are quite effective for many practical applications of low-cost GPS receivers.

6. Conclusion

In this paper, an efficient compensation method to eliminate the effects of abrupt clock jumps appearing in low-quality GPS receivers was proposed. It was explained that abrupt clock jumps appear differently due to different clock steering methods adopted by receivers. To deal with the clock jumps that affect both the time offset and the clock bias, which are interchangeable with the opposite sign conventions, the proposed compensation method consists of two steps against the reception time misalignment and the transmission time misalignment. During the compensation of the reception time misalignment, apparent non-zero time offset values are removed and the discrepancy in the pseudorange and carrier phase jumps is rectified. During the compensation of the transmission time misalignment, large differences in line-of-sight vectors caused by satellite position differences are compensated.

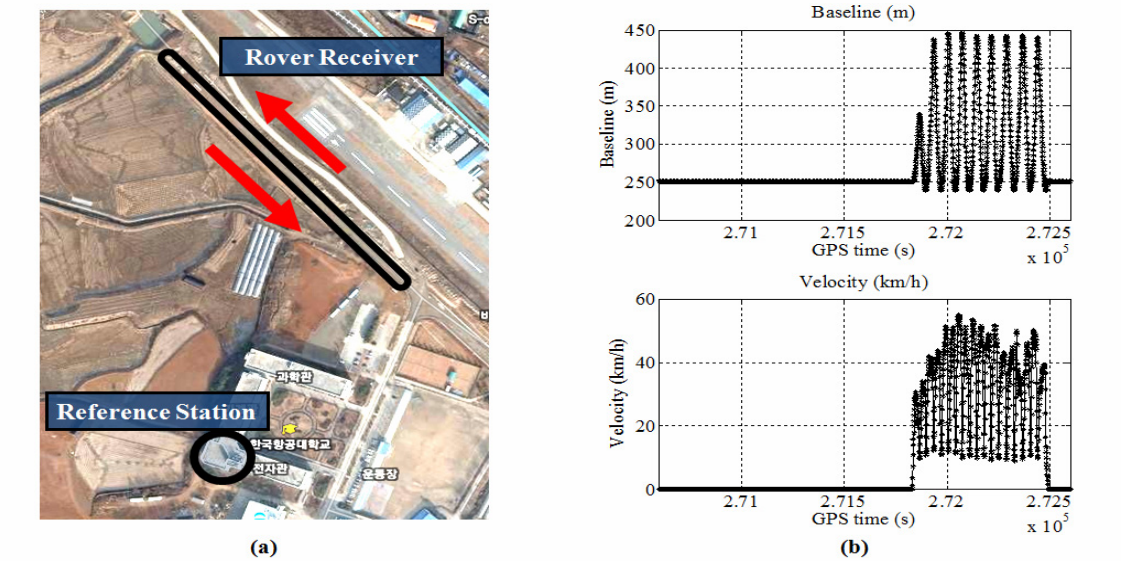

Fig. 13. Kinematic experiment: (a) Experiment area; (b) Baseline & Velocity trends

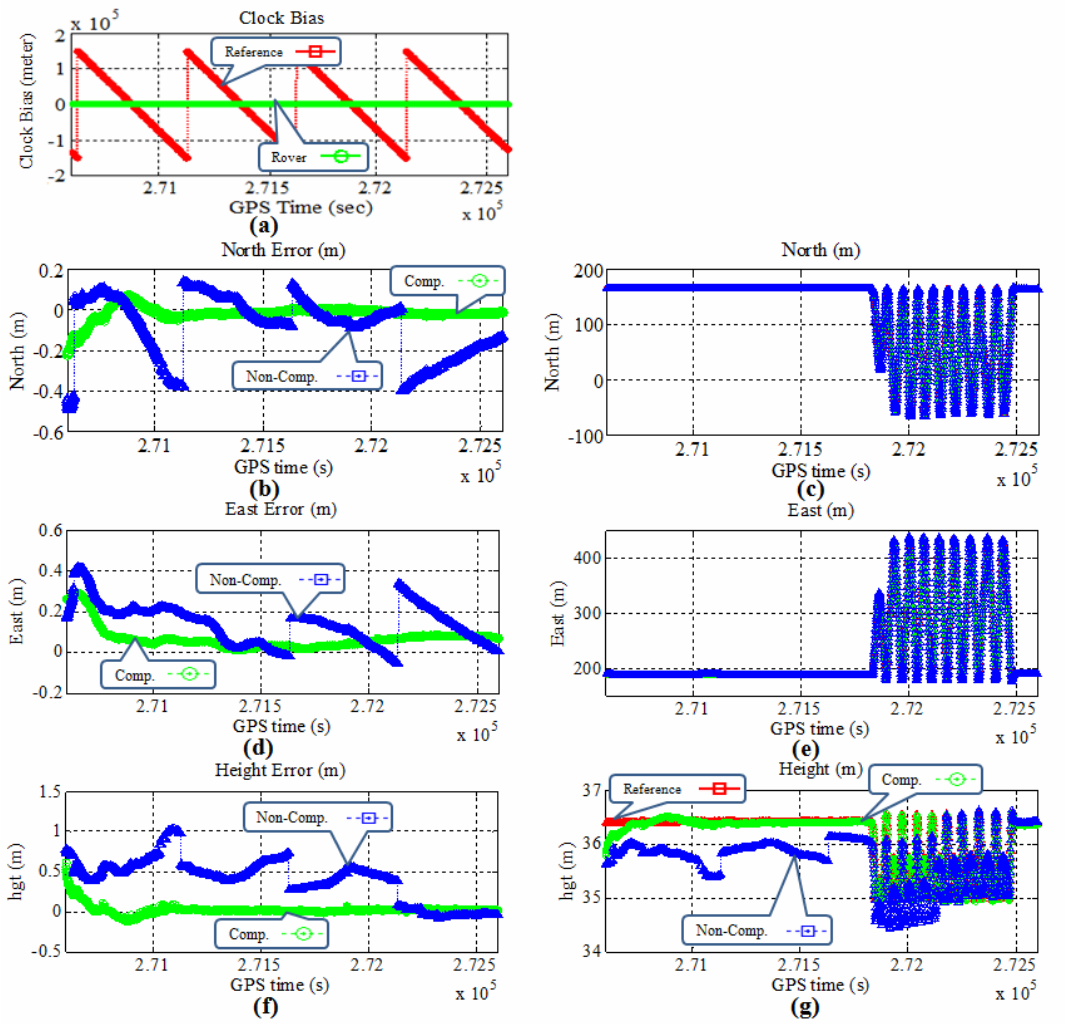

Fig. 14. Kinematic baseline experiment: (a) clock bias; (b), (d) and (e) NED error distances; (c), (g) and (f) NED trajectories

By three different experiments, it was shown that the proposed compensation method is quite effective in eliminating the undesirable clock jumps effects (Table 4).

Table 4. 3-D RMS errors in three different experiments

	3-D RMS Error (m)		
Experiment	1	2	3
Non-Compensated	1.810	0.546	0.541
Compensated	0.011	0.098	0.117

Acknowledgments

This research was supported by a grant from Transportation System Innovation Program (TSIP) funded by Ministry of Land, Transport and Maritime Affairs of Korean government.

References

[1] T. K. Yeh, C. Hwang, G. Xu, C. S. Wang, and C. C. Lee, "Determination of global positioning system (GPS) receiver clock errors: impact on positioning accuracy", *Measurement Science and Technology*, vol. 20, no. 7, pp.1-7, 2009.

[2] NovAtel Inc., *OEM4 Family of Receivers User Manu-al - Vol. 2 Command and Log Reference. OM-200000-47*, rev. 12, Alberta, Canada, 2003.

[3] A. Q. Le and C. Tiberius, "GPS Standard Positioning Service how good is it?", *European Journal of Navigation*, vol. 1, no. 2, pp.21-27, 2003.

[4] Septentrio, *PolaRx2/2e User Manual*, rev. 0, Jan. 2007.

[5] H. S. Kim and H. K. Lee, "Compensation of Time Alignment Error in Heterogeneous GPS Receivers", *Proceedings of IAIN World Congress*, Stockholm, Oct. 2009.

[6] D. Odijk, J. Traugott, G. Sachs, O. Montenbruck, and C. Tiberius, "Two Approaches to Precise Kinematic GPS Positioning with Miniaturized L1 Receivers", *ION GNSS 2007*, Fort Worth, TX, Sep. 2007.

[7] G. Werner, *RINEX The Receiver Independent Exchange Format Version 2.10*, ftp//igscb.jpl.nasa.gov/igscb/-data/format/rinex210.txt, 2001.

[8] Y. Andres and O. Montenbruc, "Kalman-filter-based GPS clock estimation for near real-time Positioning", *GPS Solutions*, vol. 13, no. 3, pp.173–182, 2009.

[9] W. P. Bradford and J. S. James, *Global Positioning System: Theory & Applications I*, AIAA, pp.121-124, 410-411, 1996.

[10] H. K. Lee and C. Rizos, "Position-Domain Hatch Filter for Kinematic Differential GPS/GNSS", *IEEE Tr. Aerospace and Electronic Systems*, vol. 44, no. 1, pp. 30-40, 2008.

Hee-Sung Kim He received the B.S. and M.S degrees in the School of Electronics, Telecommunication & Computer at Korea Aerospace University, Korea, in 2007 and 2009, respectively. He is a doctoral course student at Navigation and Information Systems Lab., Korea Aerospace University. His research interests include satellite navigation systems, GPS/GNSS network and estimation theory.

Hyung-Keun Lee He received the B.S. and M.S. degrees in control and instrumentation engineering and the Ph.D. degree from the School of Electrical Engineering and Computer Science from Seoul National University, Korea, in 1990, 1994, and 2002, respectively. Since 2003, he has been with the School of Electronics, Telecommunication and Computer Engineering at Korea Aerospace Univ., Korea, as an associate professor. His research interests include navigation systems, avionics, and estimation theory.